TEMPERATURE-RELATED PERFORMANCE OF A DIELECTRIC ELASTOMER GENERATOR WITH CONSIDERATION OF VISCOELASTICITY AND FAILURE MODES

Shoue Chen[1], Zhicheng He[1,2] and Eric Li[3]

[1] State Key Laboratory of Advanced Design and Manufacturing for Vehicle Body, Hunan University, Changsha, 410082, P. R. China (chenshoue725@163.com)

[2] State key Laboratory of Mechanical System and Vibration, Shanghai Jiaotong University, Shanghai, 200240, P. R. China (hezhicheng815@163.com)

[3] Department of Mechanical and Automation Engineering, The Chinese University of Hong Kong, Shatin, NT, Hong Kong, China (ericsg2012@gmail.com)

Keywords: Dielectric elastomer generator (DEG), Temperature, Viscoelasticity, Current leakage, Failure modes

ABSTRACT

As a smart material, the dielectric elastomer (DE) with electrodes coated on both surfaces has the capacity for converting the electrical energy into mechanical energy, vice versa. Owing to the large deformation caused by relatively small stimulations, this polymer is competent to the function of a generator. Research on dielectric elastomer generators (DEGs) has gained wide attention lately. The recent studies have proved that the electromechanical response of the DE membrane is affected by temperature, viscoelasticity and current leakage. However, very few works account for these factors simultaneously when analyzing the DEG. Therefore, in this study, on the basis of a specific compound four-stroke conversion cycle, the performance of a dissipative DEG made of very-high-bond (VHB) elastomer is investigated in detail at different temperatures. The performance parameters in this work involve the energy density as well as the conversion efficiency. Meanwhile, the mechanisms of typical failures are considered with the influence of temperature to make sure that the generator is operated in an allowable state, including loss of tension (LT), electrical breakdown (EB) and electromechanical instability (EMI). It can be observed from the numerical results that operating temperature does play a vital role in the performance of DEGs, which could possibly enhance the conversion efficiency.

1 INTRODUCTION

The dielectric elastomer (DE) often appears as a thin membrane coated with two soft electrodes on both surfaces [1, 2]. When exposure to a voltage through thickness, the DE membrane will contract in thickness and expand in area due to Maxwell stress, converting the electrical energy into mechanical energy, which is utilized as an actuator [3, 4]. The DE membrane also has the capacity for functioning as a generator owing to the large deformation induced by relatively small stimulations [5, 6]. When the membrane of DE works under certain cyclic loads, the reduction in tensile force will contribute to the enhancement in the electric potential between electrodes, converting the mechanical energy into electrical energy. There is an increasing attention on the field of dielectric elastomer generator (DEG) recently. For example, a membrane device placed behind the knee is able to recycle the energy from human motion [7], a heel-strike DEG has been implanted into shoes [8], and a wave power DEG has been developed for harvesting renewable energy [9].

Based on the fundamental property of DE, the DEG will suffer from the unavoidable dissipation processes including viscoelastic relaxation and current leakage [10]. Furthermore, some failure modes such as loss of tension (LT), electrical breakdown (EB), and electromechanical instability (EMI) may

affect the normal operating of the DE devices [11-14]. As a result, it is of great importance to research the mechanisms of failure for advanced development of DEGs. In addition, the majority of the past studies on the electromechanical performance of DE ignored the influences of temperature. However, according to the previous experiments on very-high-bond (VHB) elastomers [15-17], the permittivity and viscoelastic relaxation time of DE are strongly dependent on temperature. The shear modulus of the membrane is also proved to be related with temperature and the specific relationship should not be described by the simple T/T_0 factor anymore. To the authors' best knowledge, there is few research on the effect of temperature on the electromechanical performance of DEGs.

In this study, the most widely-used material, VHB 4910, which has high conversion efficiency and is able to produce a large deformation within a wide temperature range (233~363 K) [16] is selected to study the effect of temperature on the performance of DEGs. For the first time, an integrated model for dissipative (viscoelasticity and current leakage) DE involving the temperature-related permittivity, viscoelastic relaxation time and shear modulus is established to simulate the energy harvesting. Then, the mechanism of a four-stroke conversion cycle is introduced and applied to the DEG. By setting the cyclic stretch and the magnitudes of voltages in advance, the electromechanical responses of the DEG can be plotted at various temperatures, based on which different energies together with the conversion efficiency can all be calculated. By comparing the numerical results at different temperatures, one can summarize the effects of temperature on the performance of DEGs. At the same time, common failure modes including EB, LT and EMI are taken into consideration to ensure the allowable states, which also vary with the operating temperature.

2 MODELING FOR THE DISSIPATIVE DEG

A thin membrane of DE is sandwiched between two electrodes with negligible electrical resistance and mechanical stiffness, like conductive carbon grease. Subject to an equal-biaxial force P in plane and a voltage Φ through thickness, the membrane will deform from its original shape $L\times L\times H$ to the current shape $l\times l\times h$ with opposite charges $\pm Q_p$ gathered on the electrodes at a fixed temperature T, as sketched in Fig.1. Dielectric elastomer is assumed to be ideal and undergo homogeneous deformation. Thus, the stretch in plane can be described by $\lambda=l/L$ and the stretch in thickness is denoted by λ^{-2} due to the incompressibility of DE [1, 18]. The nominal stress in plane is defined as $s=P/(LH)$ and the nominal electric field and the nominal electric displacement are represented by $\tilde{E}=\Phi/H$ and $\tilde{D}=Q_p/L^2$, respectively.

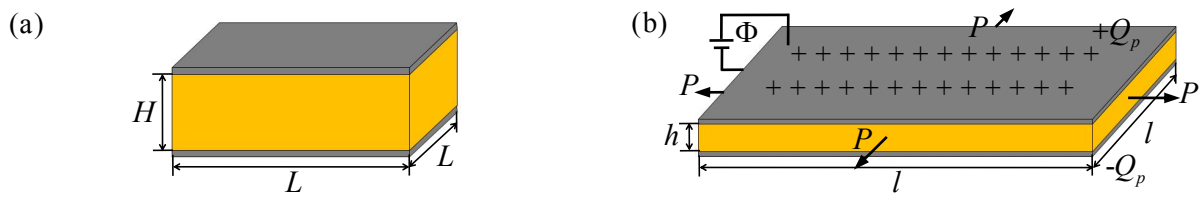

Figure 1: Schematic of the DE membrane in (a) undeformed state; (b) deformed state, subject to an equal-biaxial force in plane and a voltage through thickness at a fixed temperature *T;*

Both viscoelastic and dielectric relaxations in the DE membrane are induced by local movements of molecules. However, the deformation caused by the rotation of dipoles is negligible compared to that caused by polymer chains stretching. Also, the dielectric relaxation time is orders of magnitude smaller than viscoelastic relaxation time for VHB elastomer [19]. As a result, the dielectric relaxation can be omitted. According to the recent studies, the viscoelastic relaxation is simulated by a nonlinear rheological model [20-22], as shown in Fig.2a. The model consists of two parallel networks: spring A in parallel with spring B and a dashpot with a viscosity η. Factors μ^A and μ^B depict the shear moduli of the springs and are functions of temperature, J_A and J_B are dimension parameters referring to the dependence on chain extension limits of the elastomer. In this study, it is assumed that J_A and J_B are independent of temperature.

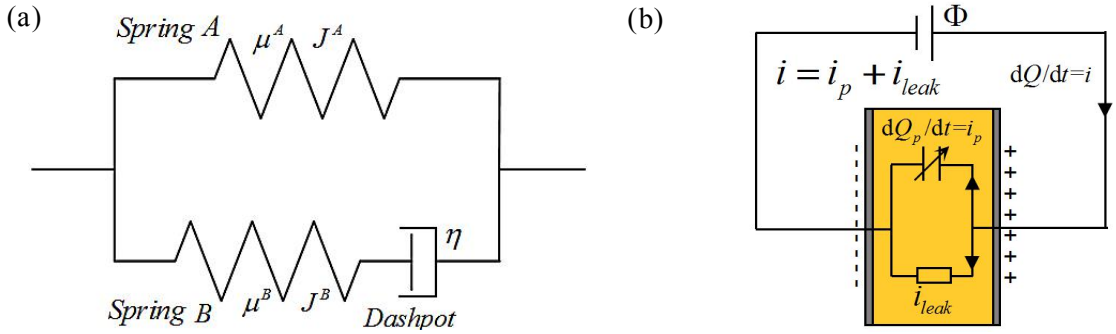

Figure 2: Dissipation processes: (a) rheological model for viscoelasticity; (b) current leakage model.

In the rheological model, the stretch of DE λ equals the net stretches in both networks: for spring A, the stretch in it is just λ. While the stretch in spring B is represented by λ^e, which cooperates with the inelastic stretch ξ in the dashpot. A well-established rule [10] is used to connect these stretches, $\lambda=\lambda^e\xi$. To measure the mechanical work done by the dashpot, that is, the viscous loss during the harvesting, the stress condition in the rheological model should also be figured out. Subject to mechanical forces in plane and a voltage through thickness, the membrane will be actuated by the stress arising form the force σ_{force} and the Maxwell stress $\sigma_{Maxwell}$. The total external stresses are balanced by the stresses in both networks, $\sigma^A+\sigma^B=\sigma_{Maxwell}+\sigma_{force}$, where the stress in the top network σ^A equals the stress in spring A, and the stress acting on the dashpot is the same as the stress in spring B, which is also the stress in the bottom network σ^B.

The Helmholtz free energy of DE is described by the sum of the Helmholtz free energy associated with the elastomer stretching and polarization. On account of the strain-stiffening effect induced by finite configurations of the polymer chains [23], the Gent model [24] is employed to characterize the Helmholtz free energy associated with deformation. The Helmholtz free energy associated with the polarization is denoted by $D^2/(2\varepsilon)$, where D is the electric displacement and ε is the permittivity of DE. The latter research has indicated that the permittivity of DE will be affected by temperature and stretch [16], which also confirms to the molecular physics: molecules contain more thermodynamic energy at a higher temperature and the stretch will alter the active range of the molecules, resulting in a greater amplitude of random thermal motion. Then the molecules are less closely aligned with each other and the permittivity declines [23]. The relative permittivity for VHB 4910 can be fitted as $\varepsilon_r=a\lambda^2+b/T+c$, where a describes the electrostriction, b is determined by $M\eta_d^2/(3\kappa\varepsilon_0)$ (M, η_d and κ represent the dipole current density, dipole moment and Boltzmann constant, respectively) and c is the relative permittivity at the reference state. The specific Helmholtz free energy is illustrated in Eq.(1).

$$W=-\frac{\mu^A(T)J^A}{2}\ln\left(1-\frac{2\lambda^2+\lambda^{-4}-3}{J^A}\right)-\frac{\mu^B(T)J^B}{2}\ln\left(1-\frac{2\lambda^{-2}\xi^{-2}+\lambda^{-4}\xi^4-3}{J^B}\right)+\frac{\tilde{D}^2}{2\varepsilon_0(a\lambda^2+b/T+c)}\lambda^{-4} \tag{1}$$

where the shear moduli of the springs satisfy the relationship $\mu^A/\mu^B=3/7$ [10] and the instantaneous modulus of DE is defined as $\mu(T)=\mu^A+\mu^B=Y(T)/3$, where $Y(T)$ denotes the isothermal elastic modulus in small deformation at temperature T. A set of parameters for VHB 4910 are chosen as: $J^A=90$, $J^B=30$ [25] and $Y(T)=0.2001(1000/T)^2-1.078(1000/T)+1.518$ MPa [15]. In addition, $\varepsilon_0=8.85\times10^{-12}$ F/m is the vacuum permittivity and the parameters for the relative permittivity are a=-0.0533 F/m, b=645.4224 F.K/m and c=3.1834 F/m [16].

When the electrodes are connected to an electric power source through a conducting wire, charges will be activated and transferred from one electrode to another, making potential difference between the surfaces. Essentially, dielectric elastomer functions as a dielectric medium between two compliant electrodes plates and the DEG is a stretchable plane-parallel capacitor. Thus, the additional charges on

the DEG can be stored or released through an electric circuit along with the deformation induced by mechanical forces. The governing equation for a capacitor is $Q_p=\Phi C$, where C is the capacitance. By definition, the electric displacement is $D=Qp/(\lambda L)^2$, and electric field is $E=\Phi/h$. These two variables can be related by $D=\varepsilon_0\varepsilon_r E$ can be illustrated in Eq.(2).

$$Q_P = C\Phi = \left[\frac{L^2}{H}\varepsilon_0(a\lambda^6+\frac{b}{T}\lambda^4+c\lambda^4)\right]\Phi \tag{2}$$

As an electrical component, the DEG will definitely suffer from unavoidable leakage problem. As sketched in Fig.2b, the leaked current i_{leak} can be modeled by a conductor which is in parallel with a capacitor. The experiment has proved that the conductivity of the VHB elastomer rises exponentially with the increasing electric field, $j_{leak}=\sigma_0\exp(E/E_B)E$, where $j_{leak}=i_{leak}/(\lambda L)^2$ is the density of the leaked current, σ_0 denotes the conductivity under the low electric fields, and E_B is an empirical constant with the same dimension as the electric field [26]. The leaked current can be acquired from Eq.(3).

$$\frac{i_{leak}}{L^2} = \sigma_0\exp(\frac{\tilde{E}\lambda^2}{E_B})\tilde{E}\lambda^4 \tag{3}$$

where $\sigma_0=3.32\times10^{-14}$ S/m, $E_B=40$ MV/m are chosen for the following analysis. [27]

According to the non-equilibrium thermodynamics [1, 12], when the system is in mechanical and electrostatic equilibrium, the nominal stress and nominal electric field can be obtained by $s=\partial W/(2\partial\lambda)$ and $\tilde{E}=\partial W/\partial\tilde{D}$, respectively. With elimination of $\tilde{D}$, the governing equation is illustrated in Eq.(4).

$$\frac{P}{LH} = \frac{\mu^A(T)(\lambda-\lambda^{-5})}{1-(2\lambda^2+\lambda^{-4}-3)/J^A} + \frac{\mu^B(T)(\lambda\xi^{-2}-\lambda^{-5}\xi^4)}{1-(2\lambda^2\xi^{-2}+\lambda^{-4}\xi^4-3)/J^B} - \tilde{E}^2\varepsilon_0(1.5a\lambda^2+\frac{b}{T}+c)\lambda^3 \tag{4}$$

A function $F(\lambda)$ that characterizes the elasticity of the DE membrane can be achieved from Eq.(4), as illustrated in Eq.(5). In the absence of voltages, the function $F(\lambda)$ corresponds to the nominal stress $P/(LH)$. Without mechanical forces, the membrane of DE will also deform when subject to a voltage. This kind of deformation is caused by Maxwell stress, which is equivalent to an equal-biaxial nominal stress $(1.5a\lambda^2+b/T+c)\lambda^3\varepsilon_0\tilde{E}^2$. Furthermore, the ordinal items in Eq.(5) represent the nominal stresses of the top and bottom networks, respectively.

$$F(\lambda) = \frac{\mu^A(T)(\lambda-\lambda^{-5})}{1-(2\lambda^2+\lambda^{-4}-3)/J^A} + \frac{\mu^B(T)(\lambda\xi^{-2}-\lambda^{-5}\xi^4)}{1-(2\lambda^2\xi^{-2}+\lambda^{-4}\xi^4-3)/J^B} \tag{5}$$

The dashpot in the rheological model is regarded as a Newtonian fluid, so the rate of deformation can be described by $\xi^{-1}\mathrm{d}\xi/\mathrm{d}t$, and the relationship between the stretch and inelastic stretch is described in Eq.(6). The dashpot will dissipate the mechanical energy with a relaxation time $\tau(T)=\eta/\mu^B(T)$ [10]. According to the experiment data from Sheng et. al [17], the viscoelastic relaxation time at different sampling temperatures are: $\tau(273\mathrm{K})=87.216$ s, $\tau(293\mathrm{K})=72.377$ s, $\tau(313\mathrm{K})=67.802$ s, $\tau(333\mathrm{K})=65.573$ s and $\tau(353\mathrm{K})=64.747$ s.

$$\frac{\mathrm{d}\xi}{\mathrm{d}t} = \frac{\mu^B(T)}{6\eta}\frac{\lambda^2\xi^{-1}-\lambda^{-4}\xi^5}{1-(2\lambda^2\xi^{-2}+\lambda^{-4}\xi^4-3)/J^B} \tag{6}$$

3 MECHANISMS OF ENERGY CONVERSION AND FAILURE MODES

Various categories of conversion processes such as constant charge, constant voltage and constant electric [28, 29] have been designed and investigated, and the mechanisms of the conversion cycles can be summarized as: the electrical energy is extracted from a four-stroke cycle by the variable capacitance of DE. In this study, a Carnot-shape conversion cycle [30, 31] consisting of two constant

voltage processes and two open circuit processes is employed to reveal the temperature effects on the DEG. In addition, the mechanisms of common failures are discussed and feasibility of the applied loads will be verified.

3.1 energy conversion cycle

The Carnot-shape conversion cycle can be realized via a three-way switch, as illustrated in Fig.3a. A switch can connect the electrodes to the power sources with high or low voltages, or keep the membrane in an open circuit. The mechanism of an ideal four-stroke cycle is sketched in Figs.3b and c, where a contour denotes a cycle and a line is a process. In the process A→B as shown in Fig.3c, the amount of the charges on the electrodes provided by the low-voltage battery increases from Q_{low} to Q_{high} due to the augment in the capacitance (the continuous stretch of DE from λ_A to λ_B, as outlined in Fig.3a). In the process B→C, with constant charges, the voltage between the electrodes will rise when the capacitance declines (the stretch is partly released from λ_B to λ_C). Expression $\Phi_{low}C(\lambda_B)=\Phi_{high}C(\lambda_C)$ can be used to determine the extent of release. In the process C→D, the charges on the electrodes are pumped to the high-voltage battery due to the further decline in the capacitance (the stretch decreases from λ_C to λ_D). Finally, in the process D→A, with charges maintained again, the voltage between the electrodes will decline when the capacitance enhances (the stretch increase from λ_A the initial state). In this cycle, the mechanical force pumps a certain amount of charges from the low-voltage battery to the high-voltage battery.

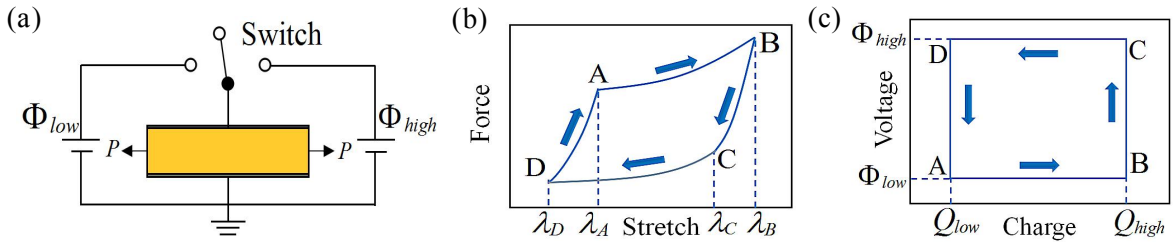

Figure 3: The mechanism of an ideal four-stroke cycle: (a) the circuit that enables the DEG to convert the mechanical energy into electrical energy; (b) (c) the force-stretch and voltage-charge diagrams in a complete cycle.

The past research has indicated that the pre-stretch can enhance the stability and produce a larger nominal electric field [32]. So the DEG is pre-stretched with an initial stretch λ_0 before stimulation. In the process A→B, subject to a low-voltage battery Φ_{low}, the DEG is stretched by a equal-biaxial force from λ_0 to λ_{max}. In the process B→C, the battery disconnects, and the DEG is partly released from λ_{max} to λ_c. In the process C→D, a high-voltage battery is applied and the force releases further to make the stretch decline to λ_{min}. In the process D→A, the force stretches the DEG back to the initial state under open circuit condition. For simplicity, the stretch rate $|d\lambda/dt|$ in each process is constant. As described before, the viscoelastic relaxation time will influence the time for DE to attain stability, so the period of the conversion cycle should be set around τ to make the DEG be steady sooner. In the simulation, the period for constant voltage process is 30 s and that for open circuit process is 6 s. The initial, maximum and minimum stretches are set as λ_0=4.5, λ_{max}=6 and λ_{min}=4.2. The time-dependent stretch in a single cycle is plotted in Fig.4a. Turn to electrical part, the nominal electric fields of the DEG in constant voltage processes are constants (Φ_{low}/H=1.8 kV/mm in A→B, Φ_{high}/H=3 kV/mm in C→D). While in open circuit processes, the nominal electric field should be calculated from Eq.(2) and will exhibit a slight temperature dependence because of the b/T factor. It is assumed in this study that the processes of charge and discharge of the DEG at states C and A will be accomplished in no time, so the nominal electric field can attain Φ_{high}/H and Φ_{low}/H instantaneously. The nominal electric field as a function of time and temperature in a single cycle is plotted in Fig.4b with the enlarged views around 36 s and 72 s.

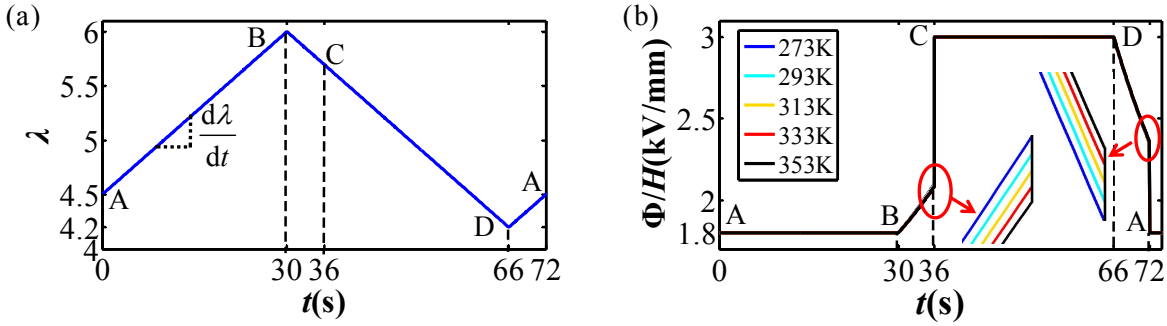

Figure 4: (a) the cyclic stretch for the energy conversion; (b) the nominal electric field for the DEG at different temperatures;

3.2 failure modes

Before studying the performance of the DEG, mechanisms of failures should be researched at first to ensure that the DEG operates under allowable conditions with the applied cyclic loads [31]. In this section, the mechanisms of electrical breakdown (EB), loss of tension (LT) and electromechanical instability (EMI) are discussed in detail and the feasibility of the cycle is validated. Material rupture is ignored as the membrane will not be stretched to the extension limit of the polymer, as suggested by the previous experiment, λ_R=6 for VHB 4910 under equal-biaxial state [33].

As a kind of dielectric material, the DE membrane will suffer from electrical breakdown when the electric field keeps increasing. Recently, the electrical breakdown field is proved to be related with the stretch [34] and can be fitted to the existing experimental data, as shown in Eq.(7).

$$\tilde{E}_{EB} = E_{EB}(\lambda)\lambda^{-2} = E_{EB}(1)\lambda^{R-2} \tag{7}$$

where $E_{EB}(1)$ denotes the electrical breakdown field in the reference state and the exponent coefficient R measures the sensitivity of the field toward the stretch. A set of parameters for VHB 4910 is chosen: $E_{EB}(1)$=30.6 MV/m and R=1.13 [13].

Keeping the membrane in tension has great importance, as wrinkles will be induced easily by any compressive planar stress. The critical condition for LT is s=0. Vanishing the nominal stress in Eq.(4), the critical nominal electric field for LT is obtained in Eq.(8). In addition, subject to a voltage, the DE membrane will shrink in thickness and contribute to a higher true electric field. The positive feedback between the true electric field and the thickness may make the membrane thin down sharply, resulting in EMI. The critical condition for EMI is determined as: when the equal-biaxial force is fixed, the voltage becomes a function of stretch. The peak of Φ(λ) corresponds to the critical condition for EMI. Differentiate Eq.(4) with respect to stretch, the critical nominal electric field for EMI can be derived in Eq.(9).

$$\tilde{E}_{LT}^2 = \frac{\dfrac{\mu^A(T)(\lambda-\lambda^{-5})}{1-(2\lambda^2+\lambda^{-4}-3)/J^A} + \dfrac{\mu^B(T)(\lambda\xi^{-2}-\lambda^{-5}\xi^4)}{1-(2\lambda^2\xi^{-2}+\lambda^{-4}\xi^4-3)/J^B}}{\varepsilon_0(1.5a\lambda^2+b/T+c)\lambda^3} \tag{8}$$

$$\tilde{E}_{EMI}^2 = \frac{\left(\begin{array}{l}\dfrac{\mu^B(\lambda\xi^{-2}-\lambda^{-5}\xi^4)(4\lambda\xi^{-2}-4\lambda^{-5}\xi^4)}{\left(1-(2\lambda^2\xi^{-2}+\lambda^{-4}\xi^4-3)/J^B\right)^2 J^B} + \dfrac{\mu^A(\lambda-\lambda^{-5})(4\lambda-4\lambda^{-5})}{\left(1-(2\lambda^2+\lambda^{-4}-3)/J^A\right)^2 J^A} \\ + \dfrac{\mu^B(\xi^{-2}+5\lambda^{-6}\xi^4)}{\left(1-(2\lambda^2\xi^{-2}+\lambda^{-4}\xi^4-3)/J^B\right)} + \dfrac{\mu^A(1+5\lambda^{-6})}{\left(1-(2\lambda^2+\lambda^{-4}-3)/J^A\right)}\end{array}\right)}{(7.5a\lambda^4+3b\lambda^2/T+3c\lambda^2)\varepsilon_0} \tag{9}$$

The cyclic stretch in Fig.4a is substituted into the above equations to achieve the critical nominal electric fields for the failures mentioned. The critical condition for EB is independent of temperature and the minimum critical value is 8.78 kV/mm, which is larger than Φ_{high}/H. The critical boundaries for LT and EMI vary with temperature and a higher temperature corresponds to a smaller nominal electric field, which can be observed from Fig.5. Based on the numerical results, the minimum critical value for LT is 4.15 kV/mm and that for EMI is 5.17 kV/mm. The lowest boundaries for these two failures are above the nominal electric field applied in Fig.4b as well. In summary, the conversion cycle will not lead to any failures within the temperature range from 273 to 353 K.

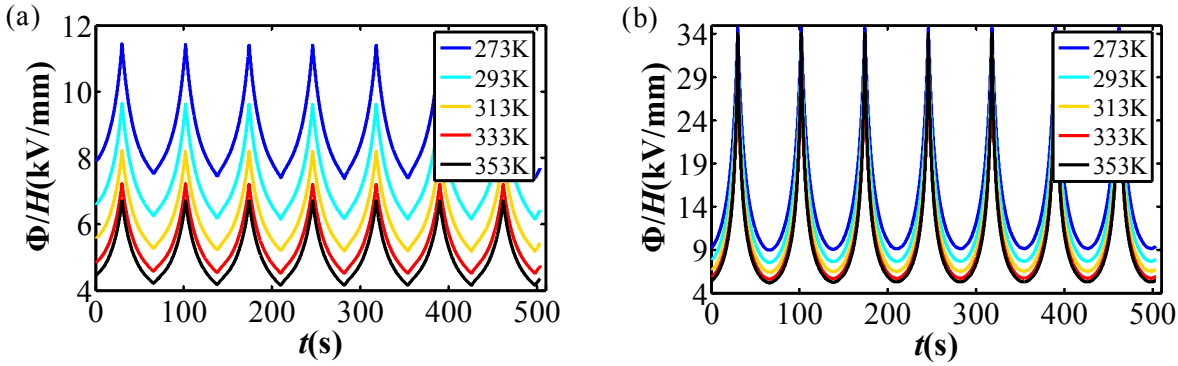

Figure 5: The critical boundaries at different temperatures for (a) loss of tension (LT); (b) electromechanical instability (EMI);

4 EFFECTS OF TEMPERATURE ON THE DEG

Due to viscoelastic relaxation, the polymer chains will not attain stable configurations instantly. As a result, it will take the DEG some time (several cycles) to obtain stable mechanical parameters such as inelastic stretch and nominal stress (the relevant parameters will get steady after the first six cycles). The inelastic stretch can be acquired from Eq.(6) once the stretch is defined. The inelastic stretches under various temperatures are plotted in Fig.6. It is found a higher temperature contributes to a larger inelastic stretch, however, the effect of temperature on the inelastic stretch will get smaller in high temperature range (the curves of inelastic stretch at 333 and 353 K are very close). In addition, the peak of the inelastic stretch in every single cycle does not correspond to the peak of the stretch and the maximum inelastic stretch will never exceed λ_{max}. Substitute the stretch and inelastic stretch into Eq.(4), the temperature-dependent nominal stress can be plotted in Fig.7 and the curves indicate the DEG requires a larger equal-biaxial force to satisfy the operating condition in the conversion cycle at a lower temperature, which can be explained by the smaller modulus induced by higher temperature.

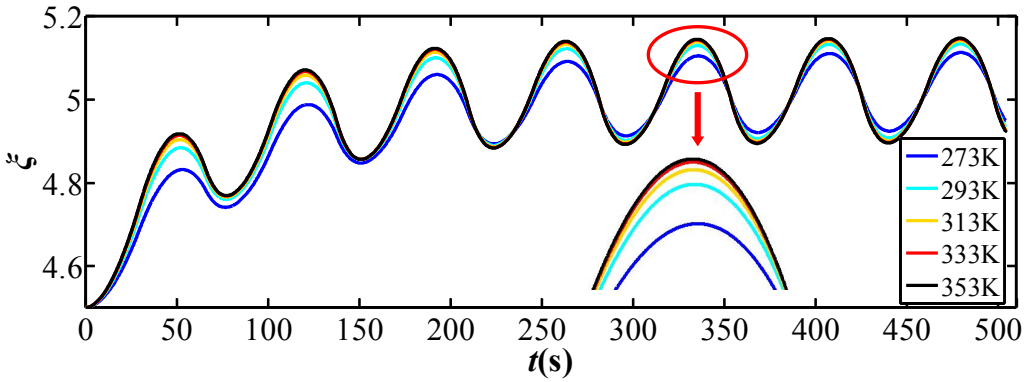

Figure 6: The inelastic stretch as a function of time at different temperatures.

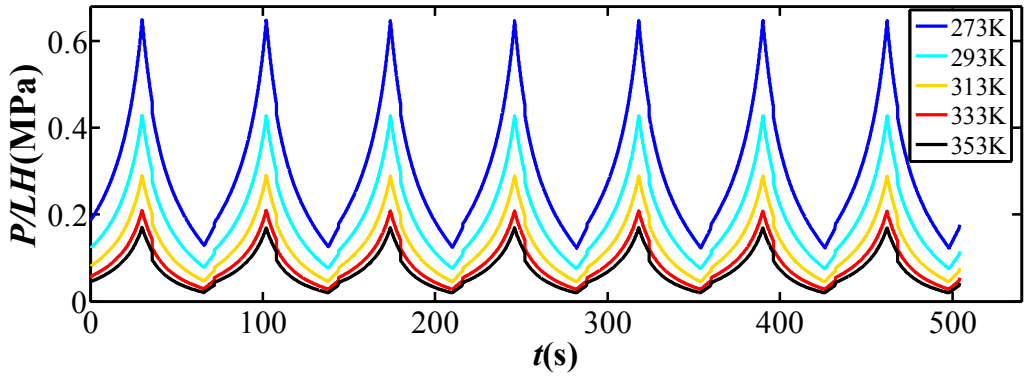

Figure 7: The nominal stress as a function of time at different temperatures.

The amount of the charges on the electrodes $\pm Q_p$ can be calculated from Eq.(2) and varies with temperature because of the temperature-related capacitance and nominal electric field. The amount of leaked charges can be solved by the integral of i_{leak} which also depends on temperature. The amounts of the charges Q_p and Q_{leak} at various temperatures are illustrated in Figs.8a and b, and these variables will attain steady state in the first conversion cycle due to the absence of ξ. From the curves, a higher temperature will induce smaller amounts of Q_p and Q_{leak} mainly because of the smaller capacitance, and the maximum value will appear at state C in every single cycle. The total amount of leaked charge will increase after every single cycle due to the periodicity of the applied loads. The total amount of the charges through the wire is acquired by the addition of Q_p and Q_{leak}.

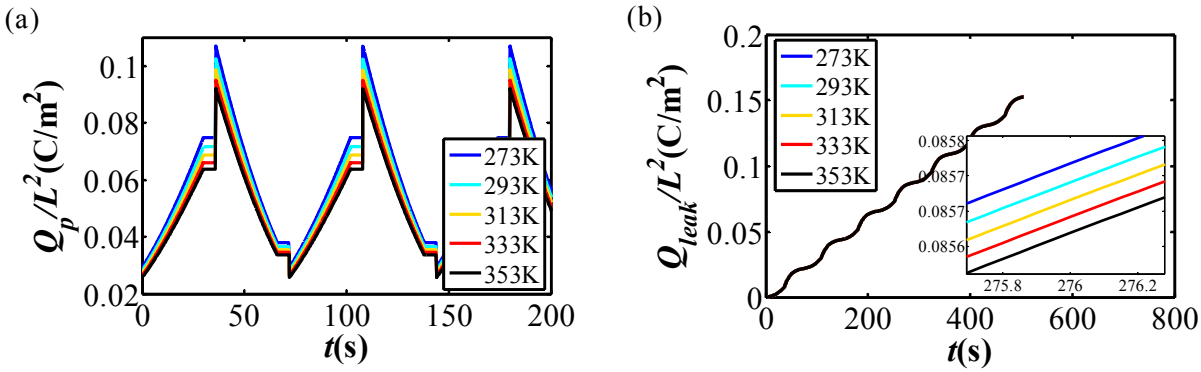

Figure 8: The amount of the charges as a function of time at different temperatures (a) on the electrodes; (b) dissipated by leakage.

Based on the condition of the energy flow in the conversion, we can regard the mechanical work done by the equal-biaxial force as the absolute input part Q_{mech}, the energy dissipated by the inelastic stretch and leaked current as the loss part $Q_{visc+}Q_{leak}$, and the difference between the electrical energy pumped to the high-voltage battery and the electrical energy absorbed from the low-voltage battery as the absolute output part Q_{ele}. The electro-mechanical conversion efficiency of the DEG is acquired by α=1-(w_{visc}+w_{leak})/w_{mech}, where the density of the mechanical energy is calculated by $w_{mech}=2\int P/(HL)\mathrm{d}\lambda$, the density of the viscous loss is given as $w_{visc}=2\int s^B\mathrm{d}\xi$, and the density of the electrical loss is $w_{leak}=\int(\Phi/H)\mathrm{d}(Q_{leak}/L^2)$. It is obvious that the conversion efficiency operates at α=1 without losses, and the DEG will have a negative efficiency if the amount of the energy lost is larger than the mechanical energy, resulting in no energy harvested. Meanwhile, the electrical energy containing the electrical energy generated and the energy dissipated by the leaked current is obtained by $w_{pele}=-\int(\Phi/H)\mathrm{d}(Q_p/L^2)$ for verification. The relevant variables are chosen from the steady-state (the seventh cycle in Figs.6-8) and the $P/(LH)$-λ diagram, the s^B-ξ diagram, the Φ/H-Q_{leak}/L^2 diagram and the Φ/H-Q_p/L^2 diagram are demonstrated in Fig.9 with temperature variation.

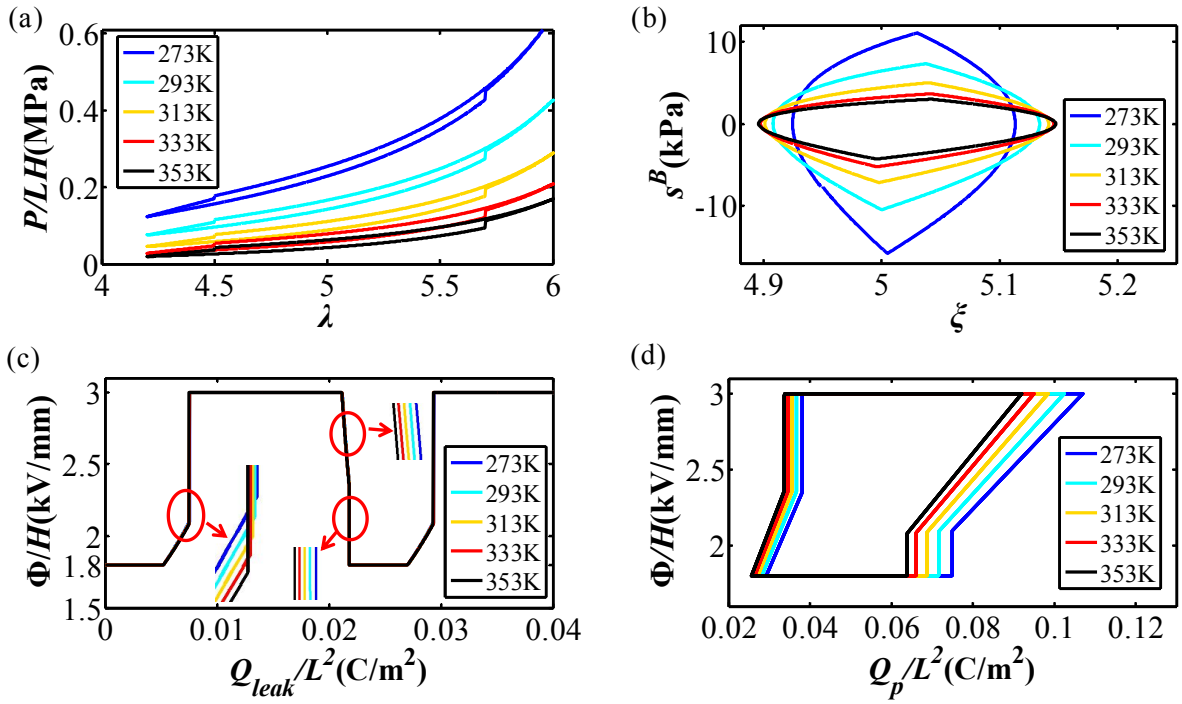

Figure 9: The curves characterize energies at different temperatures: (a) the mechanical energy produced by the force; (b) the energy dissipated by viscoelasticity; (c) the energy loss due to current leakage; (d) the total electrical energy;

The values of these energy densities at different sampling temperatures are listed in the following table. It is found in the second column that the mechanical energy decreases with a higher temperature, and the temperature tends to have less influence on the mechanical energy (the difference of w_{mech} is 0.4291 J/m^3 from 273 to 293 K and 0.2482 J/m^3 from 333 to 353 K). The third column shows that the DEG dissipates less mechanical energy at a higher temperature. These phenomena are mainly caused by the smaller shear modulus at higher temperature. When temperature rises, the electrical energy lost will be slightly reduced because of the lower nominal electric field in process B→C and D→A, as is seen from the fourth column. It is clear in the fifth column that a higher conversion efficiency can be realized when the DEG is working at a lower temperature and the conversion efficiency will even get negative when the operating temperature is relatively high (313~353 K). The reason is that lowering the temperature contributes to more mechanical energy than the the energy dissipated. The electrical energy which has the same trend as the mechanical energy is listed in the last column. Furthermore, it is observed that the mechanical energy w_{mech} is almost equal to the sum of the energy dissipated w_{visc} and the electrical energy w_{pele} that includes the energy lost by leakage w_{leak} and the absolute output part, satisfying the conservation of energy.

T (K)	w_{mech} (J/m^3)	w_{visc} (J/m^3)	w_{leak} (J/m^3)	α	w_{pele} (J/m^3)
273	6.7736e+04	6.6292e+03	5.6528e+04	6.76%	6.1106e+04
293	6.3445e+04	5.2668e+03	5.6511e+04	2.63%	5.8178e+04
313	5.9475e+04	3.8487e+03	5.6494e+04	-1.46%	5.5626e+04
333	5.6291e+04	2.9095e+03	5.6479e+04	-5.50%	5.3381e+04
353	5.3809e+04	2.4183e+03	5.6465e+04	-9.43%	5.1390e+04

Table 1. Energy densities and conversion efficiency at different temperatures.

5 CONCLUSIONS

In this study, with consideration of the major dissipation processes including viscoelasticity and current leakage and the temperature-dependent permittivity, shear modulus and viscoelastic relaxation time, a comprehensive model focusing on the influences of temperature on the performance of DEGs is proposed. On the basis of a specific energy conversion cycle, the performance parameters including the energy density and conversion efficiency are fully figured out at various temperatures. It is noticed the DEG operates more efficiently at lower temperature owing to the relatively more enhancement in the input mechanical energy than the viscoelastic loss. Furthermore, the failure modes are discussed at different temperatures to ensure the normal operation of the DEG. It is also observed that the DEG will suffer from LT and EMI more easily at higher temperature. The simulation in this study may offer help and guideline in the design and optimization of energy harvesting under different temperature conditions, which can contribute to a more efficient dissipative DEG.

ACKNOWLEDGEMENTS

The authors wish to thank the support of National Natural Science Foundation of China (Grant No.61232014) and Project funded by China Postdoctoral Science Foundation. The authors also wish to thank Research Project of State Key Laboratory of Structural Analysis for Industrial Equipment (Grant No.GZ1403), Science Fund of State Key Laboratory of Advanced Design and Manufacturing for Vehicle Body (Grant No.51375001), and Research Project of State Key Laboratory of Mechanical Systems and Vibration MSV201711.

REFERENCES

[1] Z. G. Suo, Theory of dielectric elastomers. *Acta Mechanics Solids Sinica*, **23**, 2010, pp. 549-578.
[2] A. O'Halloran, F. O'Malley and P. McHugh, A review on dielectric elastomer actuators, technology, applications, and challenges. *Journal of Applied Physics*, **104**, 2008, pp. 071101.
[3] P. Brochu and Q. Pei, Advances in dielectric elastomers for actuators and artificial muscles. *Macromolecular Rapid Communications*, **31**, 2010, pp. 10-36.
[4] S. Tsuchitani, T. Sunahara and H. Miki, Dielectric elastomer actuators using Slide-Ring Material® with increased permittivity. *Smart Materials & Structures*, **24**, 2015, pp. 065030.
[5] S. J. Adrian Koh, C. Keplinger, T. F. Li and S. Bauer, Dielectric Elastomer Generators: How Much Energy Can Be Converted? *IEEE/ASME Transactions On*, **16**, 2011, pp. 33-41.
[6] R. D. Kornbluh and Q. Pei, Dielectric elastomers: generator mode fundamentals and applications. *Proceedings of SPIE*, **4329**, 2001, pp. 148-156.
[7] C. Jean-mistral, Dielectric polymer: scavenging energy from human motion. *Proceedings of SPIE*, **6927**, 2008, pp. 692716-692716-10.
[8] L. C. Rome, L. Flynn, E. M. Goldman and T. D. Yoo, Generating electricity while walking with loads. *Science*, **309**, 2005, pp. 1725-1728.
[9] S. Chiba, M. Waki, R. Kornbluh and R. Pelrine, Innovative wave power generation system using electroactive polymer artificial muscles. *Oceans IEEE*, 2009, pp. 1-3.
[10] C. Chiang Foo, S. Cai, S. J. Adrian Koh and S. Bauer, Model of dissipative dielectric elastomers. *Journal of Applied Physics*, **111**, 2012, pp. 836-382.
[11] L. W. Liu, Z. Zhang, Y. J. Liu and J. S. Leng, Failure modeling of folded dielectric elastomer actuator. *Science China Physics, Mechanics & Astronomy*, **57**, 2014, pp. 263-272.
[12] X. H. Zhao and Z. G. Suo, Method to analyze electromechanical stability of dielectric elastomers. *Applied Physics Letter*, **91**, 2007, pp. 061921.
[13] J. S. Plante and S. Dubowsky, Large-scale failure modes of dielectric elastomer actuators. *International Journal of Solids & Structures*, **43**, 2006, pp. 7727-7751.
[14] C. Keplinger, T. F. Li, R. Baumgartner, Z. G. Suo and S. Bauer, Harnessing snap-through instability in soft dielectrics to achieve giant voltage-triggered deformation. *Soft Matter*, **8**, 2012, pp. 285-288.

[15] T. Vucong, C. Jeanmistral, and A. Sylvestre. New operating limits for applications with electroactive elastomer: effect of the drift of the dielectric permittivity and the electrical breakdown. The role of migration in the history of the Eurasian steppe:.Macmillan, 2013, pp. 793-806.
[16] C. Jean-Mistral, A. Sylvestre, S. Basrour and J. J. Chaillout, Dielectric properties of polyacrylate thick films used in sensors and actuators. *Smart Materials & Structures*, **19**, 2010, pp. 075019.
[17] J. Sheng, H. Chen, L. Liu, J. Zhang, Y. Wang and S. Jia, Dynamic electromechanical performance of viscoelastic dielectric elastomers. *J. Appl. Phys.* **114**, 2013, pp. 134101-134101-8.
[18] X. H. Zhao, W. Hong and Z. G. Suo, Electromechanical coexistent states and hysteresis in dielectric elastomers. *Physics Review B*, **76**, 2007, pp. 1283.
[19] A. S. A. Reffaee, D. E. E. Nashar, S. L. Abd-El-Messieh and A. E. Nour, Electrical and mechanical properties of acrylonitrile rubber and linear low density polyethylene composites in the vicinity of the percolation threshold. *Materials & Design,* **30**, 2009, pp. 3760-3769.
[20] J. S. Zhang, L. L. Tang, B. Li, Y. J. Wang, and H. L. Chen, Modeling of the dynamic characteristic of viscoelastic dielectric elastomer actuators subject to different conditions of mechanical load. *Journal of Applied Physics*, **117**, 2015, pp. 084902.
[21] H. M. Wang, M. Lei and S. Q. Cai, Viscoelastic deformation of a dielectric elastomer membrane subject to electromechanical loads. *Journal of Applied Physics*, **113**, 2013, pp. 213508-213508-7.
[22] J. S. Zhang, H. L. Chen, L. L. Tang, B. Li, J. J. Sheng and L. Liu, Modeling of spring roll actuators based on viscoelastic dielectric Elastomers. *Applied Physics A.* **119**, 2015, pp. 825-835.
[23] B. Li, H. L. Chen, J. H. Qiang and J. X. Zhou, A model for conditional polarization of the actuation enhancement of a dielectric elastomer. *Soft Matter*, **8**, 2013, pp. 311-317.
[24] A. N. Gent, A new constitutive relation for rubber. *Rubber Chemistry and Technology* **69**, 1996, pp. 59-61.
[25] S. Michel, X. Q. Zhang, M. Wissler, C. Löwe and G. Kovacs, A comparison between silicone and acrylic elastomers as dielectric materials in electroactive polymer actuators. *Polymer international*, **59**, 2010, pp. 391-399.
[26] A. Bergamini, Dielectric and insulating properties of an acrylic DEA material at high near-DC electric fields. *Proceedings of SPIE*, **7976**, 2011, pp. 79763B-79763B-6.
[27] T. A. Gisby, S. Q. Xie, E. P. Calius and I. A. Anderson, Leakage current as a predictor of failure in dielectric elastomer actuators. *Proceedings of SPIE*, **7642**, 2010, pp. 764213-764213-11.
[28] C. Graf and J. Maas, Evaluation and optimization of energy harvesting cycles using dielectric elastomers. *Electroactive Polymer Actuators & Devices*, **7976**, 2011, pp. 541-558.
[29] C. Graf, J. Maas and D. Schapeler, Energy harvesting cycles based on electro active polymers. *Proceedings of SPIE*, **7642**, 2010, pp. 579-595.
[30] C. Chiang Foo, S. J. Adrian Koh, C. Keplinger and R. Kaltseis, Performance of dissipative dielectric elastomer generators. *Journal of Applied Physics*, **111**, 2012, pp. 836-839.
[31] S. J. Adrian Koh, X. H. Zhao and Z. G. Suo, Maximal energy that can be converted by a dielectric elastomer generator. *Applied Physics Letter*, **94**, 2009, pp. 262902-262902-3.
[32] M. Wissler and E. Mazza, Modeling of a pre-strained circular actuator made of dielectric elastomers, *Sensors and Actuators A: Physical*, **120**, 2005, pp. 184-192.
[33] P. Sommer-larsen and G. Kofod, Performance of dielectric elastomer actuators and materials. *Proceedings of SPIE*, 2002, pp. 158-166.
[34] G. Kofod, P. Sommer-larsen, R. D. Kornbluh and R. Pelrine, Actuation response of polyacrylate dielectric elastomers. *Journal of Intelligent Material Systems & Structures*, **14**, 2003, pp. 787-793.